LA-UR- LA-UR- 01-1854

Approved for public release; distribution is unlimited.

Title:	Homogeneous Infinite Media Time-Dependent Analytical Benchmarks
Author(s):	B. D. Ganapol, University of Arizona, Tucson, AZ R. S. Baker, CCS-4, LANL J. A. Dahl, CCS-4, LANL R. E. Alcouffe, CCS-4, LANL
Submitted to:	International Meeting on Mathematical Methods for Nuclear Applications, Salt Lake City, Utah, September 9-13, 2001

Los Alamos
NATIONAL LABORATORY

Homogeneous Infinite Media Time-Dependent Analytical Benchmarks

B.D. Ganapol[+]
Department of Aeorspace and Mechanical Engineering
University of Arizona
Tucson, AZ 85721

R.S. Baker, J.A. Dahl and R. E. Alcouffe
CCS-4
Los Alamos National Laboratory
Los Alamos, NM 87545

Keywords: Time-dependence, Multiple collisions, Gauss quadrature

ABSTRACT

A suite of analytical benchmarks, called **AZURV1**, has been developed for verification of time-dependent neutral particle transport algorithms in the one group approximation. Only 1-D sources in infinite media are considered. The 1-D sources include infinite plane, point, infinite line, spherical shell and solid spherical pulsed emissions. The analytical solution for each source is based on the solution to the pulsed plane source. Transformations between geometries then give scalar flux expressions to be numerically evaluated to analytical benchmark accuracy for the fundamental pulsed sources considered.

1. INTRODUCTION

This presentation is the first in a series describing analytical time-dependent benchmarks for verification and assessment of numerical time-dependent particle transport methods. Here, only conventional neutral particle transport benchmarks will be considered in a one-dimensional, one group, isotropic scattering setting. Time-dependent problems are more complex than stationary ones simply because time adds an additional dimension. For this reason, analytical time-dependent solutions to the transport equation are rare in 1-D and virtually nonexistent in multi-dimensions. Fortunately, one exceptional case, that of an infinite medium, stands out. For a 1-D homogeneous plane infinite medium, a truly remarkable time-dependent analytical solution was discovered by Monin (Monin, 1956) and expressed in a more complete form by Kholin (Kholin, 1964). It is this solution that will be exploited to provide a suite of benchmarks extended to curvilinear geometries.

2. Theory in a Plane Infinite Medium

A. Multiple Collision Expansion

In this section, the solution to the time-dependent transport equation in plane geometry,

[+] Work partially performed under ASCI research contract # 0757499199

$$\left[\frac{\partial}{\partial t}+\mu\frac{\partial}{\partial x}+1\right]\phi_{pl}(x,\mu,t)=\frac{c}{2}\int_{-1}^{1}d\mu\,\phi_{pl}(x,\mu',t)+\frac{1}{2}\delta(x)\delta(t)\ , \qquad (1a)$$

will be derived subject to the conditions

$$\lim_{|x|\to\infty}\phi_{pl}(x,\mu,t)<\infty \qquad (1b)$$

$$\phi_{pl}(x,\mu,0)=0\ . \qquad (1c)$$

Particle position is measured in mean free path [Σ^{-1}] and time is measured in mean free time [$(v\Sigma)^{-1}$] where v is the particle speed. The medium is assumed to be homogeneous and infinite and an isotropic pulse of particles is emitted at the center plane ($x = 0$) at time zero.

The solution to eqs(1) is obtained through a multiple collision decomposition of the flux $\phi_{pl}(x,\mu,t)$. Physically, the flux is viewed as composed of particles that have suffered one, two, to an infinite number of collisions. A transport equation can then be written for the transport of particles of a given collision order n whose source comes from particles of the previous order that have just collided. The source emits only uncollided particles into the medium at $x = 0$ and $t = 0$ and satisfies

$$\left[\frac{\partial}{\partial t}+\mu\frac{\partial}{\partial x}+1\right]\phi_0(x,\mu,t)=\frac{1}{2}\delta(x)\delta(t) \qquad (2)$$

$$\lim_{|x|\to\infty}\phi_0(x,\mu,t)<\infty$$

$$\phi_0(x,\mu,0)=0\ .$$

For particles that have experienced n collisions, the appropriate transport equation is

$$\left[\frac{\partial}{\partial t}+\mu\frac{\partial}{\partial x}+1\right]\phi_n(x,\mu,t)=\frac{c}{2}\int_{-1}^{1}d\mu'\phi_{n-1}(x,\mu',t) \qquad (3)$$

$$\lim_{|x|\to\infty}\phi_n(x,\mu,t)<\infty$$

$$\phi_n(x,\mu,0)=0\ .$$

The summation of all collided fluxes ϕ_n represents the entire flux at a time/space point

$$\phi_{pl}(x,\mu,t)=\sum_{n=0}^{\infty}\phi_n(x,\mu,t) \qquad (4)$$

provided the series converges which can be shown for all c (Ganapol, 1973). The scalar flux is just the angular integral of eq(4)

$$\phi_{pl}(x,t)=\sum_{n=0}^{\infty}\int_{-1}^{1}d\mu\phi_n(x,\mu,t)\equiv\sum_{n=0}^{\infty}\phi_n(x,t)\ . \qquad (5)$$

This presentation is concerned with the determination of the scalar flux to a high degree of accuracy--usually to 4 or 5 place accuracy.

The multiple collision approach seems counterintuitive with regard to mathematical elegance and simplicity. Rather than take advantage of the collective nature of the original transport equation, it is unraveled collision by collision. Mathematically, we are generating an infinite number of equations from a single equation, which seems rather

impractical. For this reason, the multiple collision approach is seldom used in the form presented here. In numerical circles, this approach is referred to as source iteration but is usually reformulated so that an approximate flux is returned at each iterate and an intervening acceleration is used to promote convergence. At this point, the theoretical advantage afforded by the multiple collision decomposition is not evident. Essentially, a single integro-differential equation is transformed into an infinite set of partial differential equations thus drastically altering the mathematical nature of the solution. As will be shown, this change has a significant theoretical advantage in that a prescription for the determination of the collided fluxes will emerge.

B. Form of the Collided Flux

By following the particle along its trajectory, the solution to eq(2) can be shown to be (Monin, 1956)

$$\phi_0(x,\mu,t)=\frac{e^{-t}}{2t}\delta(\mu-\eta) \tag{6}$$

where η is defined as the dimensionless similarity variable $\eta \equiv x/t$. This expression indicates that source particles emitted in direction μ can only have traveled a distance x/μ after a time $t = x/\mu$ has elapsed from emission. The first collided flux from eq(3) with n = 1 is found to be

$$\phi_1(x,\mu,t)=\frac{e^{-t}}{t}(ct)F_1(\mu,\eta) \tag{7}$$

with

$$F_1(\mu,\eta)\equiv\frac{1}{4}\left\{\ln\left[\frac{1+\mu}{\mu-\eta}\right]\Theta(\mu-\eta)+\ln\left[\frac{1-\mu}{\eta-\mu}\right]\Theta(\eta-\mu)\right\}\Theta(1-|\eta|)$$

where Θ is the Heaviside step function. The particular form of the solution leads conveniently to the following general form (Kholin, 1964):

$$\phi_n(x,\mu,t)=\frac{e^{-t}}{t}\frac{(ct)^n}{n!}F_n(\mu,\eta)\,. \tag{8}$$

From an involved analysis in the complex plane, each F_n can be obtained analytically; and the scalar flux can be shown to be (Ganapol, 1973)

$$\phi_{pl}(x,t)=\frac{e^{-t}}{2t}\left[1+\sum_{n=1}^{\infty}\left(\frac{ct}{2}\right)^n(n+1)Q_{n+1}^{n-1}(\eta)\right]\Theta(1-|\eta|) \tag{9a}$$

where

$$Q_{n+1}^{n-1}(\eta)\equiv\frac{\left(1-\eta^2\right)^n}{2\pi}\frac{n}{(n+1)!}\int_0^{\pi}du\sec^2\left(\frac{u}{2}\right)\mathbf{Re}\left[\frac{\ln(q)+iu}{\eta+i\tan\left(\frac{u}{2}\right)}\right]^{n+1} \tag{9b}$$

with

$$q\equiv\frac{1+\eta}{1-\eta}\,.$$

An expression for the angular flux can also be obtained, but usually is of minimal interest for benchmarking purposes.

In the past (Ganapol, 1973), eq(9a) was numerically evaluated to a high degree of accuracy; however, in order to treat more comprehensive sources, a more efficient numerical algorithm is needed since additional integrations will be required. The evaluation of eq(9a) involves a numerical integration at each collision (each n), which can be computationally expensive. The computation can be reduced to a single numerical integration by performing the summation analytically to give the following expression for the flux:

$$\phi_{pl}(x,t)=\frac{e^{-t}}{2t}\left\{1+\frac{ct}{4\pi}\left(1-\eta^2\right)\int_0^{\pi} du\sec^2\left(\frac{u}{2}\right)\mathbf{Re}\left[\xi^2 e^{\frac{ct}{2}\left(1-\eta^2\right)\xi}\right]\right\}. \quad (10)$$

with

$$\xi(u)\equiv\frac{\ln(q)+iu}{\eta+i\tan\left(\frac{u}{2}\right)}.$$

The solution given by eq(10) will now be used to construct solutions for sources in various infinite medium configurations in curvilinear geometry.

3. Theory for Spherical and Cylindrical Geometry

A. Point Source

The scalar flux from a pulsed point isotropic source is most easily obtained from the following plane/point transformation:

$$\phi_{pt}(r,t)=-\frac{1}{2\pi r}\frac{\partial\phi_{pl}(r,t)}{\partial r}. \quad (11)$$

This transformation is most simply derived from the corresponding steady state expression after a Laplace transform and inversion. It is also valid for any order anisotropic scattering but not for heterogeneous media.

With eq(11) applied to eq(9a), the scalar flux at the radius r for pulsed point source emission is (Ganapol, 1977)

$$\phi_{pt}(r,t)=\frac{e^{-t}}{4\pi rt^2}\left[\begin{array}{c}\delta(1-\eta)+(ct)\ln\left[\frac{1+\eta}{1-\eta}\right]+\\ +\sum_{n=2}^{\infty}\left(\frac{ct}{2}\right)^n(n+1)nQ_{n+1}^{n-2}(\eta)\end{array}\right]\Theta(1-|\eta|). \quad (12)$$

Again by analytically summing the series, a closed form can be obtained

$$\phi_{pt}(r,t)=\phi_{pt0}(r,t)+\phi_{pt1}(r,t)+$$

$$+\frac{1}{2\pi}\frac{e^{-t}}{4\pi rt^2}\left(\frac{ct}{2}\right)^2(1-\eta^2)\int_0^{\pi}du\sec^2\left(\frac{u}{2}\right)\mathbf{Re}\left[\left(\eta+i\tan\left(\frac{u}{2}\right)\right)\xi^3 e^{\frac{ct}{2}(1-\eta^2)\xi}\right]\Theta(1-\eta) \quad (13)$$

with the uncollided and first collided contributions given by

$$\phi_{pt0}(r,t)\equiv\frac{e^{-t}}{4\pi rt^2}\delta(1-\eta),\quad \phi_{pt1}(r,t)\equiv\frac{e^{-t}}{4\pi rt^2}(ct)\ln\left[\frac{1+\eta}{1-\eta}\right].$$

Now that the point source response has been found, it is only a matter of integration over surfaces or lines to find fluxes in other infinite geometries.

B. Shell Source

Consider the isotropic pulsed shell source of radius a shown below. If the source is normalized to q_0, a point source can be integrated over the surface of the shell to give

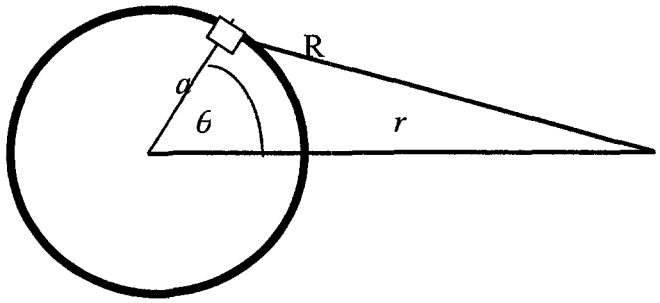

the flux at r

$$\phi_{sh}(r,t)=q_0a^2\int_0^{2\pi}d\phi\int_0^{\pi}d\theta\,\sin(\theta)\phi_{pt}(R,t)$$

with

$$R\equiv r^2+a^2-2ar\cos(\theta).$$

When R is substituted, this expression becomes

$$\phi_{sh}(r,t)=-q_0\frac{a}{r}\int_{|a-r|}^{a+r}dRR\frac{1}{2\pi R}\frac{\partial\phi_{pl}(R,t)}{\partial R}$$

$$=q_0\frac{a}{r}\left[\phi_{pl}(|a-r|,t)-\phi_{pl}(|a+r|,t)\right]. \quad (14)$$

If the shell source is normalized such that one particle/s is emitted at time zero over the entire shell, then

$$q_0\equiv\frac{1}{4\pi a^2}.$$

C. Solid Spherical Pulsed Source

To obtain the flux from a pulsed solid sphere of radius R at a point r outside the sphere, the sphere is viewed as composed of continuous shell sources (as shown below). The contribution from the internal shell sources in a differential ring are integrated over

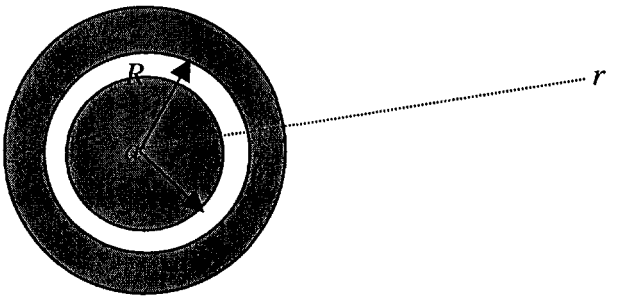

the entire sphere to obtain

$$\phi_{sp}(r,t) = q_0 \int_0^R da \frac{a}{r}\left[\phi_{pl}(|a-r|,t) - \phi_{pl}(|a+r|,t)\right],$$

or on changing variables

$$\phi_{sp}(r,t) = \frac{3}{4\pi R r}\int_0^1 d\omega\omega\left[\phi_{pl}(|R\omega - r|,t) - \phi_{pl}(|R\omega + r|,t)\right] \qquad (15)$$

where the normalization

$$q_0 \equiv \frac{4\pi R^3}{3}$$

has been imposed. Thus, to evaluate this expression, two numerical integrations are necessary, though with some manipulation one integral can be transformed into a Q-like function.

D. Infinite Line Source

The flux form an isotropically emitting infinite line source is found by integrating a point source over a line as shown below. This results in

$$\phi_l(\rho,t) = \int_{-\infty}^{\infty} dz' \phi_{pt}(r,t) \qquad (16)$$

where

$$r = \sqrt{\rho^2 + (z-z')^2}\ .$$

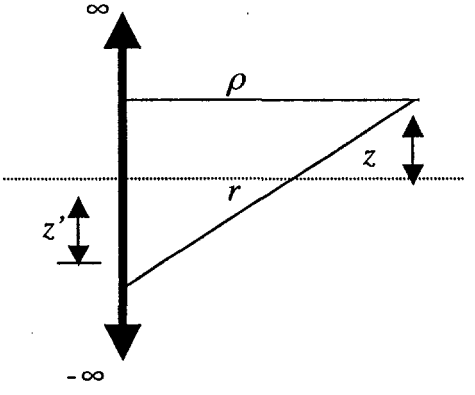

Noting that the point source flux is zero until the pulse reaches the point (ρ, z), eq(16) can be recast into the more numerically convenient form

$$\phi_l(\rho,t) = 2t\int_0^{\sqrt{1-\eta^2}} d\omega\phi_{pt}\left(t\sqrt{\eta^2+\omega^2}, t\right)\Theta(1-\eta)$$

with $\eta \equiv \rho / t$. The uncollided contribution can be extracted from the integral to give

$$\phi_l(\rho,t)=\left[\frac{e^{-t}}{2\pi t^2}\frac{1}{\sqrt{1-\eta^2}}+2t\int_0^{\sqrt{1-\eta^2}} d\omega\,\phi_{ptc}\left(t\sqrt{\eta^2+\omega^2},t\right)\right]\Theta(1-\eta)\,, \qquad (17)$$

where ϕ_{ptc} is the collided portion of the flux from a point source.

4. Numerical Implementation and Output

A. Required Numerical Methods

The primary numerical procedure required to evaluate the time behavior of the scalar flux for the above five sources is numerical quadrature. Two numerical procedures have been adapted for this purpose. The first, the evaluation of the integrals in eqs(9a) and (13), is performed using a Gauss/Legendre quadrature rule of order Lm. The integrals over either the plane or point fluxes in eqs(15) and (17) are also performed using a Legendre/Gauss quadrature rule.

The second procedure is an outer iteration on the quadrature order to ensure analytical benchmark quality accuracy. The initial quadrature order is set by the user and incremented by 2 until the solution converges to the desired accuracy. The error is estimated as the maximum difference between two iterates taken over the edit grid(s) (either time, space or both).

B. Selected Results

B.1 Plane, Point and Line Sources

The primary numerical procedure required to evaluate the time behavior of the scalar flux for the above five sources is numerical quadrature. Two numerical procedures have been adapted for this purpose. The first procedure, to evaluate the integrals in eqs(9a) and (13), uses a Gauss/Legendre quadrature rule of order L_m. The integrals over either the plane or point fluxes in eqs(15) and (17) are also performed using a Legendre/Gauss quadrature rule.

The second procedure is an outer iteration on the quadrature order to ensure analytical benchmark quality. The initial quadrature order is set by the user and incremented by 2 until the solution converges to the desired accuracy. The error is estimated as the maximum difference between two iterates taken over the edit grid(s) (either time, space or both).

Tables 1a-c present examples of convergence of the outer iteration. The plane, point and line sources are considered for a conservative ($c = 1$) medium. The initial quadrature was set at 10 and a relative error of 10^{-5} was specified. The three sources were run to convergence for positions $x = 1(1)5$ and times $t = 1(2)45$. Convergence was achieved as

Table 2: Quadrature Order for Convergence

Source	*Lm*
Plane	26
Point	34
Line	26

shown in Table 2. The values obtained, when compared to those from the evaluation of the multiple collision series [Collided Flux Expansion Method, (ganapol,1977)], differ at most by the relative error of 10^{-4} quoted for the plane and point sources. For the line source, the quoted relative error is 10^{-3}. The shaded entries are not within a relative error of 10^{-4} indicating that the original calculation was more accurate than originally thought. Only near the wave front is the line source not as accurate as the point and plane source.

B.2 Spherical Shell Source

Because of causality, the flux at a given time t will have reached a position (exterior to shell) of $x = a + r = t$ from pulsed spherical shell of radius a. The flux is shown in Fig. 1 for $a = 1$ with the flux for short times after emission shown in the top plate. For times less than 1, the pulse has not yet reached the shell center. The dotted line with the large increase at $r = 0$ is very near the time the flux first reaches the center. Note that at $t = 0.1$, the flux has reached only ± 0.1 from the point of emission ($r = 1$). The bottom plate clearly shows a "rarefaction" wave moving away from the center after the flux has become infinite. A comparison of the flux traces from a point source and solid spherical source (of radius a=1) at long times is shown in Figure 2. As expected, the spherical source appears to behave like a point source at long times

B.3 Comparison to PARTISN

The expressed purpose of the time-dependent benchmarks is to provide a sufficiently stringent test of time-dependent numerical methods. Currently, the **PARTISN** (Alcouffe,) discrete ordinates/diamond difference transport code is under development at LANL. While **PARTISN** is primarily to be used as a multi-dimensional transport code, a one-dimensional version does exist. Figure 3 shows a comparison between the analytical benchmark and **PARTISN** for an infinite cylindrical pulsed source. Excellent agreement is observed except very near the wavefront where numerical diffusion causing blurring of the front. A **PARTISN/AZUR** comparison for additional, more complicated sources, will also be performed.

References

Alcouffe,R.E., Baker, R.S., J.A. Dahl,
Ganapol,B.D, and Grossman,L.M., *NS&E*, 52,454(1973).
Ganapol,B.D.,McKenty,P.W., and Peddicord,K.L., *NS&E*, 64, 317(1977).
Monin,A.S., *Prob. Theo. & App.(USSR)*, 3 328(1956).
Kholin,S.A., *USSR Comp. Math. and Math. Phys.*, 4, 213(1964).

Table 1a: Plane Source

estimated max relative error (for lm= 26)= 9.9545E-06

t/x	1.0000E+00	2.0000E+00	3.0000E+00	4.0000E+00	5.0000E+00
1.0000E+00	1.8394E-01	0.0000E+00	0.0000E+00	0.0000E+00	0.0000E+00
3.0000E+00	2.3944E-01	9.3839E-02	8.2982E-03	0.0000E+00	0.0000E+00
5.0000E+00	1.9957E-01	1.2105E-01	4.9596E-02	1.1823E-02	6.7385E-04
7.0000E+00	1.7348E-01	1.2293E-01	6.8029E-02	2.8448E-02	8.4159E-03
9.0000E+00	1.5528E-01	1.1935E-01	7.6385E-02	4.0186E-02	1.7004E-02
1.1000E+01	1.4175E-01	1.1455E-01	7.9986E-02	4.7954E-02	2.4433E-02
1.3000E+01	1.3120E-01	1.0969E-01	8.1201E-02	5.3024E-02	3.0372E-02
1.5000E+01	1.2269E-01	1.0514E-01	8.1159E-02	5.6305E-02	3.4986E-02
1.7000E+01	1.1564E-01	1.0096E-01	8.0438E-02	5.8391E-02	3.8531E-02
1.9000E+01	1.0968E-01	9.7167E-02	7.9349E-02	5.9664E-02	4.1241E-02
2.1000E+01	1.0455E-01	9.3720E-02	7.8067E-02	6.0377E-02	4.3305E-02
2.3000E+01	1.0007E-01	9.0584E-02	7.6693E-02	6.0699E-02	4.4869E-02
2.5000E+01	9.6129E-02	8.7721E-02	7.5287E-02	6.0744E-02	4.6043E-02
2.7000E+01	9.2615E-02	8.5099E-02	7.3885E-02	6.0593E-02	4.6912E-02
2.9000E+01	8.9460E-02	8.2689E-02	7.2509E-02	6.0302E-02	4.7543E-02
3.1000E+01	8.6607E-02	8.0465E-02	7.1169E-02	5.9910E-02	4.7984E-02
3.3000E+01	8.4010E-02	7.8405E-02	6.9873E-02	5.9449E-02	4.8275E-02
3.5000E+01	8.1633E-02	7.6492E-02	6.8625E-02	5.8938E-02	4.8445E-02
3.7000E+01	7.9447E-02	7.4708E-02	6.7425E-02	5.8393E-02	4.8519E-02
3.9000E+01	7.7427E-02	7.3042E-02	6.6273E-02	5.7827E-02	4.8516E-02
4.1000E+01	7.5554E-02	7.1480E-02	6.5168E-02	5.7247E-02	4.8450E-02
4.3000E+01	7.3811E-02	7.0013E-02	6.4108E-02	5.6662E-02	4.8334E-02
4.5000E+01	7.2183E-02	6.8631E-02	6.3092E-02	5.6074E-02	4.8177E-02

Table 1b: Point Source

estimated max relative error (for lm= 34)= 9.5365E-06

t/x	1.0000E+00	2.0000E+00	3.0000E+00	4.0000E+00	5.0000E+00
1.0000E+00	6.9437E-01	0.0000E+00	0.0000E+00	0.0000E+00	0.0000E+00
3.0000E+00	2.2003E-02	1.0187E-02	1.0441E-02	0.0000E+00	0.0000E+00
5.0000E+00	1.0350E-02	6.5741E-03	2.9566E-03	8.5552E-04	5.0871E-04
7.0000E+00	6.2716E-03	4.5418E-03	2.6144E-03	1.1654E-03	3.8288E-04
9.0000E+00	4.3089E-03	3.3538E-03	2.1944E-03	1.1937E-03	5.3016E-04
1.1000E+01	3.1916E-03	2.6004E-03	1.8417E-03	1.1274E-03	5.9123E-04
1.3000E+01	2.4854E-03	2.0900E-03	1.5625E-03	1.0350E-03	6.0442E-04
1.5000E+01	2.0059E-03	1.7263E-03	1.3423E-03	9.4107E-04	5.9294E-04
1.7000E+01	1.6629E-03	1.4566E-03	1.1670E-03	8.5397E-04	5.6950E-04
1.9000E+01	1.4076E-03	1.2503E-03	1.0256E-03	7.7604E-04	5.4089E-04
2.1000E+01	1.2115E-03	1.0884E-03	9.0986E-04	7.0730E-04	5.1071E-04
2.3000E+01	1.0570E-03	9.5851E-04	8.1396E-04	6.4694E-04	4.8086E-04
2.5000E+01	9.3283E-04	8.5252E-04	7.3353E-04	5.9394E-04	4.5229E-04
2.7000E+01	8.3117E-04	7.6470E-04	6.6536E-04	5.4732E-04	4.2542E-04
2.9000E+01	7.4672E-04	6.9096E-04	6.0702E-04	5.0615E-04	4.0042E-04
3.1000E+01	6.7565E-04	6.2834E-04	5.5666E-04	4.6967E-04	3.7728E-04
3.3000E+01	6.1519E-04	5.7464E-04	5.1284E-04	4.3720E-04	3.5595E-04
3.5000E+01	5.6323E-04	5.2816E-04	4.7444E-04	4.0819E-04	3.3630E-04
3.7000E+01	5.1820E-04	4.8762E-04	4.4058E-04	3.8217E-04	3.1820E-04
3.9000E+01	4.7886E-04	4.5201E-04	4.1054E-04	3.5873E-04	3.0152E-04
4.1000E+01	4.4426E-04	4.2053E-04	3.8375E-04	3.3754E-04	2.8615E-04
4.3000E+01	4.1363E-04	3.9254E-04	3.5974E-04	3.1832E-04	2.7195E-04
4.5000E+01	3.8637E-04	3.6752E-04	3.3812E-04	3.0083E-04	2.5882E-04

Table 1c: Line Source

estimated max relative error (for lm= 26)= 9.1551E-06

t/x	1.0000E+00	2.0000E+00	3.0000E+00	4.0000E+00	5.0000E+00
1.0000E+00	4.1402E+01	0.0000E+00	0.0000E+00	0.0000E+00	0.0000E+00
3.0000E+00	7.4361E-02	3.2009E-02	6.2261E-01	0.0000E+00	0.0000E+00
5.0000E+00	4.6024E-02	2.8603E-02	1.2315E-02	3.2650E-03	3.0336E-02
7.0000E+00	3.3261E-02	2.3836E-02	1.3463E-02	5.8210E-03	1.8199E-03
9.0000E+00	2.6029E-02	2.0135E-02	1.3034E-02	6.9760E-03	3.0265E-03
1.1000E+01	2.1376E-02	1.7347E-02	1.2201E-02	7.3929E-03	3.8228E-03
1.3000E+01	1.8133E-02	1.5205E-02	1.1312E-02	7.4409E-03	4.3042E-03
1.5000E+01	1.5744E-02	1.3521E-02	1.0476E-02	7.3064E-03	4.5721E-03
1.7000E+01	1.3911E-02	1.2165E-02	9.7197E-03	7.0842E-03	4.6998E-03
1.9000E+01	1.2460E-02	1.1053E-02	9.0465E-03	6.8239E-03	4.7367E-03
2.1000E+01	1.1282E-02	1.0125E-02	8.4493E-03	6.5516E-03	4.7150E-03
2.3000E+01	1.0308E-02	9.3393E-03	7.9191E-03	6.2809E-03	4.6558E-03
2.5000E+01	9.4893E-03	8.6659E-03	7.4470E-03	6.0193E-03	4.5731E-03
2.7000E+01	8.7907E-03	8.0825E-03	7.0250E-03	5.7700E-03	4.4761E-03
2.9000E+01	8.1878E-03	7.5723E-03	6.6462E-03	5.5346E-03	4.3711E-03
3.1000E+01	7.6624E-03	7.1224E-03	6.3047E-03	5.3135E-03	4.2620E-03
3.3000E+01	7.2002E-03	6.7228E-03	5.9955E-03	5.1062E-03	4.1518E-03
3.5000E+01	6.7907E-03	6.3654E-03	5.7144E-03	4.9122E-03	4.0423E-03
3.7000E+01	6.4252E-03	6.0441E-03	5.4579E-03	4.7306E-03	3.9347E-03
3.9000E+01	6.0971E-03	5.7535E-03	5.2230E-03	4.5606E-03	3.8298E-03
4.1000E+01	5.8008E-03	5.4895E-03	5.0071E-03	4.4014E-03	3.7281E-03
4.3000E+01	5.5320E-03	5.2487E-03	4.8080E-03	4.2520E-03	3.6299E-03
4.5000E+01	5.2870E-03	5.0280E-03	4.6240E-03	4.1119E-03	3.5352E-03

Fig. 1 Spherical Shell Source ($a = 1$)

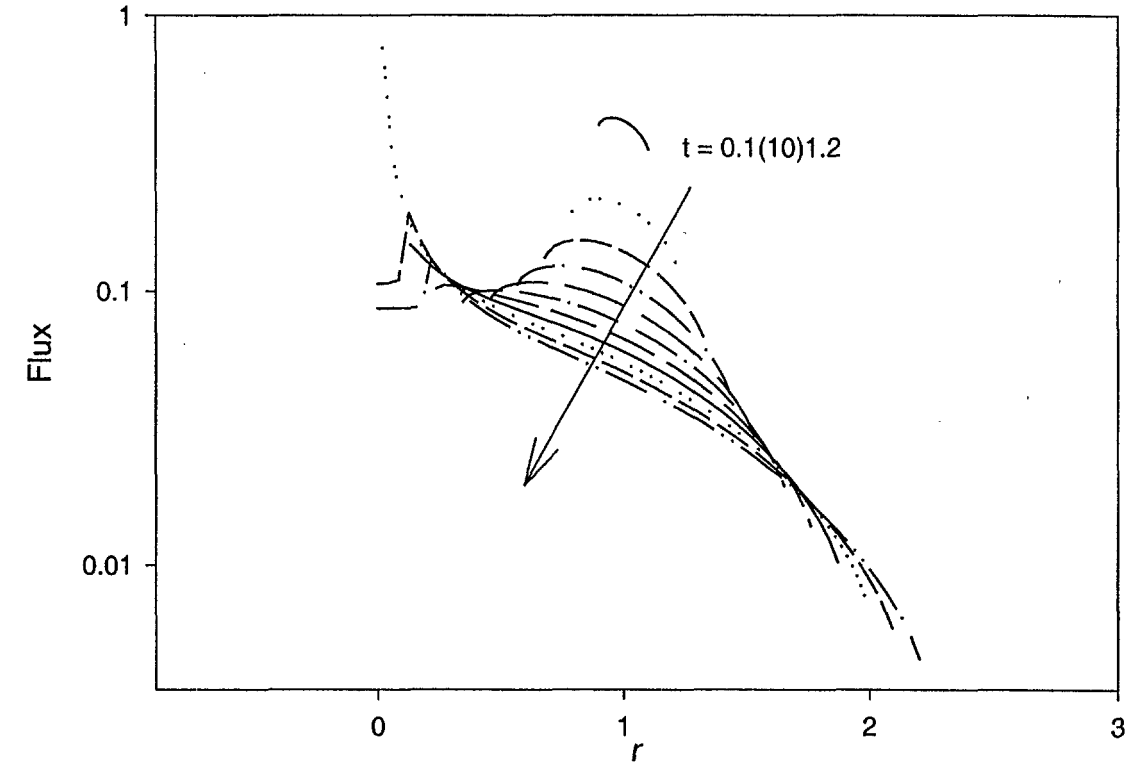

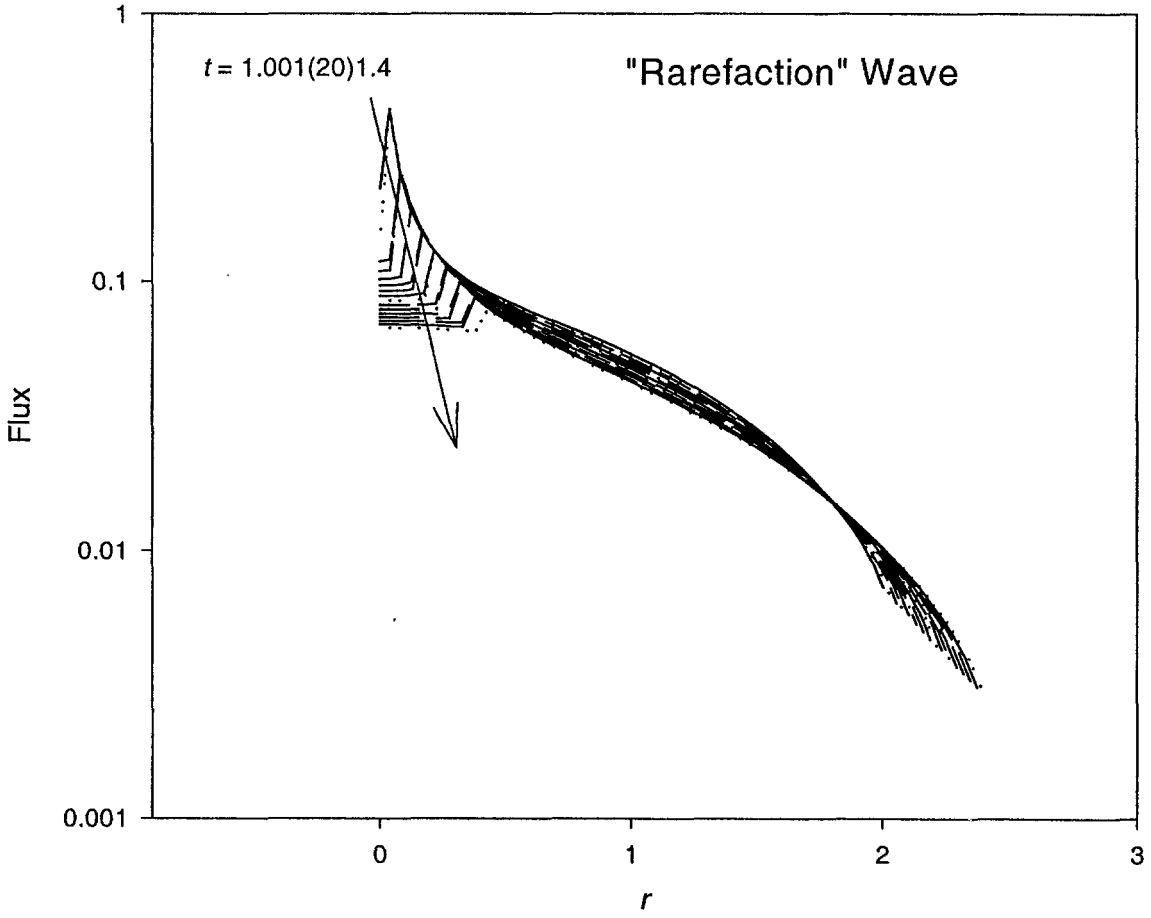

Fig. 2: Comparison of Point and Spherical Sources (trace)

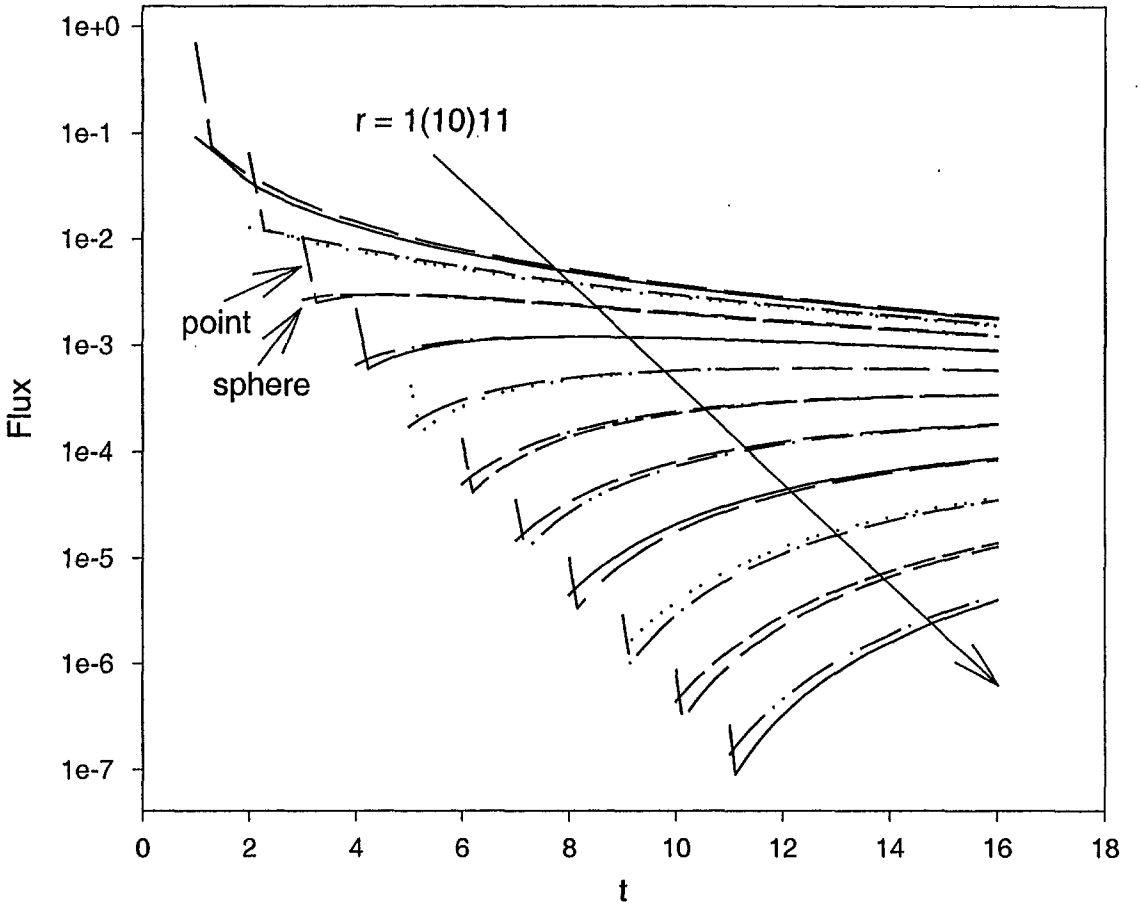

Figure 3 Comparison of **PARTISN** and **AZURE** for a cylindrical source